Proceedings of the 3rd International Conference on
Vortex Flows and Vortex Models (ICVFM2005)
Yokohama, JAPAN, November 21 - 23, 2005

A Vortex Method for Simulating Three-Dimensional Turbulent Flows

Peter S. Bernard
Department of Mechanical Engineering, University of Maryland
College Park, Maryland 20742, U.S.A. / Email bernard@umd.edu

Jacob Krispin
VorCat, Inc.
Rockville, Maryland 20850, U.S.A. / Email jacob@vorcat.com

Key Words: turbulent flow, vortex methods

ABSTRACT

The advent of fast numerical solutions to the *N*-body problem such as the Fast Multipole Method has raised the possibility of vortex method simulations of fluid flow using millions of vortex elements. This resolution is sufficient to make credible large eddy simulations of turbulent flow via vortex methods. This paper presents a particular hybrid formulation of such a scheme in which freely convecting vortex tube elements are used in conjunction with a thin, fine grid of triangular prisms adjacent to solid surfaces. The latter provides an efficient and accurate representation of the critical vortex generation process that plays a large part in the dynamics of turbulent flow. Some examples of the application of the methodology to boundary layer and bluff body flows arr given.

1. INTRODUCTION

The accuracy of numerical simulation schemes for turbulent flow depends in large measure on satisfactorily resolving critical flow processes involving the development and dynamics of vortices. This is particularly important near solid boundaries where vorticity production for the whole flow usually takes place and where energetic vortical structures of many scales are produced that generate Reynolds shear stress and otherwise control the flow physics.

It is the hallmark of Direct Numerical Simulation (DNS) that the computed turbulent field is resolved completely in the sense that all vortical features are resolved free of the smearing that would occur if the numerical grid were not fine enough to prevent numerical diffusion. Traditional grid-based Large Eddy Simulation (LES) schemes, on the other hand, use subgrid-scale models for the purpose of capturing the gross effect on the resolved turbulence scales of largely unseen vortical motions. How this is done near boundaries is particularly important and a major factor in whether the calculations succeed or fail. For reasons unrelated to the phenomenon that is being modelled, (e.g. numerical stability) subgrid models tend to be diffusive and there is much evidence to suggest that this leads to serious distortions of the underlying turbulence. For example, the smoothing away of shed vortices and the inability to fully capture backscatter.

Vortex methods avoid the problem of grid induced numerical diffusion by eliminating the grid altogether (Puckett, 1993). Such Lagrangian methods use translating and interacting vortical elements to represent the flow field, and by so doing sharp features such as intense vortices and shear layers remain sharp as they evolve over time. This is true regardless of whether resolution is sufficient to encompass all important scales of motion. Moreover, nothing in the approach prevents the occurrence of backscatter if it should be locally present in the flow. Other advantages of vortex methods are their inherent efficiency in modelling vortical objects and their need to cover just the support of the vorticity field and not the often larger support of the velocity field.

That the near-wall region must be treated carefully in gridbased LES also holds true for vortex methods. In fact, since the vortical elements in a vortex method originate at boundaries it is particularly important to correctly compute the degree and nature of vorticity production at solid surfaces. For turbulent flow at high Reynolds number large vorticity gradients associated with vorticity production at the surface are confined to $0 \leq y^+ \leq 30$. An important point is that while this region may be very thin, it still has structure that needs to be resolved in order to accurately estimate the rate of production of vorticity and the appearance of new vortices. This means that the complete physics of the vorticity field including viscous vorticity diffusion, convection and stretching must be computed accurately next to boundaries even in a vortex method.

This paper describes the development and application of a vortex method that is specifically designed for turbulent flow simulation. In this, vortex tubes are taken as the principal gridfree element, but these are supplemented by sheet-like triangular prism vortices covering the viscous sublayer adjacent to solid boundaries in a fixed arrangement several layers deep. Upon the mesh the full 3D vorticity equation is solved by a finite volume scheme with new vortex tube elements appearing at the outer edge of the wall mesh. The attention paid to the near-wall flow reflects the necessities of the physics and may be contrasted with vortex methods that model the turbulent boundary layer via a single layer of sheets. The present hybrid scheme aims to provide accuracy and efficiency in resolving the near wall flow without eliminating the essentially gridfree character of the approach.

The following contains a brief introduction to the gridfree algorithm followed by results of its application to turbulent boundary layer and bluff body flows.

2. NUMERICAL ALGORITHM

2.1 Tubes

The vortex tube elements used in the method are straight segments defined by the positions of their end points and their circulation, Γ. By convecting the end points according to the local velocity, the changes in length and orientation of the tubes provide an approximation to the vortex stretching term in the vorticity equation. Since the focus of the method is on turbulent flow, the approximation is made that Kelvin's theorem can be applied to justify keeping the circulation of the tubes constant in time. Explicit modeling of viscous diffusion is included for the flow adjacent to the boundary in the context of the vortex sheet prisms.

The vortex tubes have a tendency to increase in length as they evolve. Tubes longer than a threshold are subdivided. Moreover, a bound is placed on $\Gamma\,\Delta s$ where Δs is the length of a tube with the consequence that vortices with large circulation are allowed to subdivide more quickly than weaker vortices. This step is found to enhance the accuracy of the discretization since $\Gamma\,\Delta s$ appears in the Biot-Savart law for the velocities produced by the tubes. As time passes, individual vortex tubes lengthen into chains of tubes that form filaments that mimic elongated vortices in turbulent flow. Very often multiple filaments are seen to form even larger organized structures. The allowable length of tubes for the most part establishes the resolution of the simulation. Usually this length is tied to the average size of the triangular elements used to represent solid surfaces.

New vortex tubes are created at the top sheet mesh with circulation determined by the local vorticity that has convected and diffused from the surface. Under turbulent flow conditions, the tubes stretch and fold as part of the fundamental mechanism of the cascade by which energy passes from large to small scales (Bernard and Wallace, 2002; Chorin, 1994). In practical terms the number of tubes grows rapidly so that, in fact, a de facto subgrid scale model is needed to limit the number of tubes. Removal of acutely folded tubes eliminates local energy that may be viewed as destined to ultimately be dissipated by viscosity at smaller scales. This is the hairpin removal procedure developed by Chorin (1993). In a similar vein, volume conservation implies that the implied radii of the tubes diminish as they stretch and subdivide. When a particular tube has divided through many generations, it can be expected that the dissipation scale has been reached and there is justification for removing such vortices from the calculation.

2.2 Prisms

Solid surfaces are represented via triangularizations. By projecting normally from the triangle nodes a thin grid of triangular prism sheets is erected. The number of layers is generally taken to be 11, and the thickness of the sheets is more or less determined for a given Reynolds number by the desire to cover the region out to $y^+ = 30$. As the Reynolds number increases, the horizontal density of triangles needs to increase if the aspect ratio of the sheets is not to get large. In fact, keeping the aspect ratio near ten is a beneficial goal since it allows for a reasonably fine coverage of sheets while still retaining the efficiency implicit in a sheet-like representation of the high vorticity next to surfaces. Moreover, the number of prisms near the wall, according to classical scaling arguments, grows with Reynolds number proportional to $R_e^{3/2}$ since the number of layers is fixed, so there is significant potential for efficiency in accommodating high Reynolds number flows.

Piecewise constant vorticity is assumed over the prisms and a finite volume scheme is applied to the 3D viscous vorticity equation to update vorticity values in time. The non-slip boundary condition gives the surface vorticity from the computed velocities using a finite difference approximation that is accurate if the sheet layer is thin enough. Typically this requires $\Delta y^+ \approx 3$ if 11 layers are to extend to $y^+ = 30$. If the triangles have aspect ratio 10 then the spanwise spacing of triangles is near 30 which is sufficient to capture the physical spacing of coherent vortices near a solid wall.

In the finite volume scheme, the convection term in conservative form is rewritten via the divergence theorem as a sum of fluxes through the five sides of the prisms. The vorticity on the triangular faces is from the upwind prism while linear least square fitting of upwind vorticity is used to compute vorticity on the quadrilateral faces. The stretching term uses the vorticity at the center of the prisms. Velocity gradients are computed using the scalar divergence theorem similar to the convection term. The evaluation of the diffusion term distinguishes between diffusion normal and parallel to the surface. For the former a standard second order finite difference formula is used while the latter is evaluated by differentiation of a polynomial determined by a second order least-square fit of the vorticities of prisms located within a given radius of the prism center and in the layers immediately above and below the prism.

At the outer level of the mesh it is necessary to both supply a boundary condition for the finite volume scheme as well as calculate the amount of vorticity to be put into new tubes. The former is satisfied by solving the finite volume equations only up to the second to last sheet level and assuming the viscous flux in the wall normal direction to be constant over this sheet. In this, when the convective flux is toward the surface the vorticity in the top sheet is taken to be zero since it may be assumed that the incoming vorticity is in the form of vortex tubes. The total vorticity flux due to convection and diffusion into the top sheet level supplies the vorticity that is put into new tubes. The orientation of the new tube corresponds to that of the vorticity, its length is determined by the dimensions of the prism and its strength is such as to guarantee far field consistency with the velocity field produced by the prism.

Time integration on the mesh is via an explicit scheme with time step, Δt, limited by CFL conditions in the normal and tangential directions as well as a diffusive stability requirement. In practice Δt satisfying these conditions is smaller than needed for accurate computation of the tube motion. Consequently, several iterations of the finite volume scheme are performed before updating the positions of the vortex tubes. The contribution of the vortex tubes to the velocities in the mesh is held fixed during the sub-iterations.

The finite volume algorithm described here is found to offer stable solutions to the 3D vorticity equation over a wide range of flows that have been treated thus far. Moreover, tests have shown each separate part of the numerical discretization to be consistent and convergent under mesh refinement.

2.3 Velocity Evaluation

The velocity field is recovered by summing over individual contributions from vortex tubes and prisms as given by the appropriate form of the Biot-Savart law plus a potential flow that insures satisfaction of the non-penetration condition at solid surfaces. The latter is determined using a boundary element method over the triangles used to describe the fixed surfaces. In the case of tubes, following the common procedure for vortex methods, a smoothing function is used to desingularize the Biot-Savart kernel. This is not necessary for the prisms since the exact 3D integration is done in this case.

The far field contribution from the prisms is done using the standard Biot-Savart kernel.

A parallel implementation of the Fast Multipole Method (FMM) (Greengard and Rokhlin, 1987) is used to evaluate all except local contributions of tubes and prisms to the velocity field. Local smoothing of the tube formula prevents growing the oct-tree in the FMM to optimal depth, but this is efficiently compensated for by use of a "middleman" scheme incorporating 3D linear interpolation over a mesh grown through two further subdivisions. Local sheet contributions are done by direct evaluation of the exact formulas.

The FMM reduces the nominal $O(N^2)$ cost of velocity evaluation for N vortices to a more practical $O(N \log(N))$ or even O(N) calculation. With 4 million vortices, excellent parallel scalability is maintained through at least 16 processors, with scalability increasing as the number of vortices increases. In a typical result, a calculation with 4 million vortices on 64 processors takes under 1 minute of CPU time. This is sufficient to enable useful simulations of complex flows in a reasonable time.

3. NUMERICAL RESULTS

Validation of the gridfree methodology has focused on comparing quantitative and qualitative predictions of a variety of flows against physical experiments and DNS. A high priority has been the turbulent boundary layer whose mean properties such as velocities and Reynolds stress are well documented. Among other flows of interest are the spatially growing mixing layer, the flow past a sphere and finite cylinder, and generic mini-van flows used in the automobile industry, namely, the Ahmed body shown in Fig. 1 (Ahmed, 1984) and the Morel body (Morel, 1978).

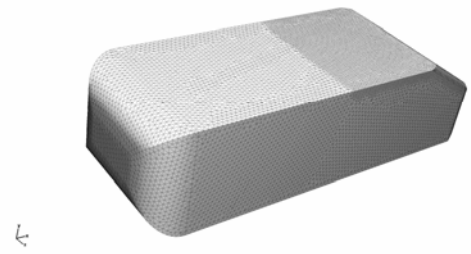

Figure 1. Ahmed body showing surface triangularization.

Among the options for studying the turbulent boundary layer, it has proven easiest to compute the flow past three-dimensional objects having flat surfaces such as a finite-thickness plate with rounded edges and the top and bottom surfaces of the Ahmed and Morel bodies. Such calculations do not require the imposition of spanwise periodicity and downstream boundary conditions as would be the case, for example, in computing the flow past an infinite flat plate. In fact, to enforce periodicity when the velocity is computed from vorticity using the Biot-Savart law, requires adding many periodic spanwise images of the vortex elements in order to recreate the complete vorticity field that influences the velocity in the computational domain. Special care also has to be taken to compensate for the contributions to the velocity from vorticity that has convected past the downstream boundary.

In the current version of the code, typical calculation with the vortex method using 16 or 32 processors on parallel computers can be completed in a matter of a few days so long as the number of surface triangles is kept below 40,000 (implying ≈ 400,000 prisms) and the number of tubes is no more than several million. With these constraints on resolution, only relatively modest Reynolds numbers can be considered if the surface mesh is to be kept near optimal conditions. More specifically, calculations at Reynolds numbers above $O(10^5)$ can be expected to be significantly under-resolved next to the boundary if only 40,000 surface triangles are used. For example, such computations tend to have grids with aspect ratio near 20, thickness $\Delta y^+ \approx 6$ and spanwise spacing on the order of 100 in wall units.

3.1 Velocity Statistics

Velocity statistics for several flows are given here at various Reynolds numbers up to 500,000. The higher Reynolds number calculations, though they have fairly coarse meshes, are performed to enable more realistic comparisons with physical experiments. For example, experimental measurements of the Ahmed body flow are at R_e = 2,784,000 based on body length. Fig. 2 is a comparison of the mean velocity scaled in wall coordinates as computed from the flat surfaces of a Morel body with square back at Re = 360,000 compared to DNS (Spalart, 1988) and the classic scaling laws. For the DNS, R_θ = 500 while for the present simulation R_θ = 622. The accuracy of the calculation is apparent as well as its consistency with the log law behavior. For this simulation the average spanwise mesh spacing is Δz^+ = 107.2. Calculations at coarser meshes than this show degradation in accuracy.

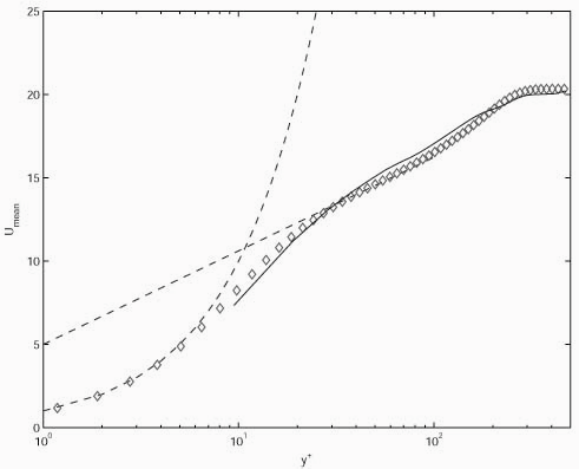

Figure 2. $\overline{U}^+$ at R_e=360,000. ◊, DNS (Spalart, 1988); —, gridfree scheme; - -, $\overline{U}^+ = y^+$ and $\overline{U}^+ = 1/0.41 \log(y^+) + 5$.

The normal Reynolds stresses for the boundary layer at R_e = 360,000, shown in Fig. 3, are somewhat over predicted. This trend is at least partly attributable to the coarseness of the wall mesh, since with better resolution the normal Reynolds stresses are better predicted. For example Figs. 4 and 5 show Reynolds stress and turbulent kinetic energy predictions for a better resolved simulation at R_e = 64,800 using the finite flat plate with rounded edges. Here the calculation has the very low value of R_θ = 146 while the DNS is at R_θ = 300. The Reynolds shear stress is well predicted while the kinetic energy has the right amplitude but peaks further from the wall. It may also be noticed that the normal stresses are somewhat too isotropic, a tendency that is also present at the higher Reynolds number. The disagreements with DNS shown in Figs. 4 and 5 can be explained by a number of factors including lingering coarseness in the wall mesh, the differences between the finite and infinite plates and the small simulation Reynolds number that is below

the minimum for a log law. Another possibility that is being investigated is a local effect of the changeover from sheet-like to tube-like behavior when new vortex tubes are created.

Measurements of velocity components and other statistics for the Ahmed body flow are well documented (Lienhart, et al., 2000) and provide another avenue with which to quantitatively check predictions. Results are given here for a calculation at R_e = 500,000 containing an inviscid ground plane in the same position as the floor in experiments. The streamwise velocity is compared with experiments in Fig. 6 for different locations along the centerline of the roof (x =0 is the front and x=1 is the back), in Fig. 7 at some transverse locations over the rear slanted window, and on the wake centerline in Fig. 8. Figure 9 shows the mean velocity normal to the top surface at the same locations as in Fig. 6. These plots show that many details of the flow are well modeled, such as the acceleration of the fluid over the top surface and the boundary layer profiles over the rear window. It is interesting to note that the profile at z = 0.21073 in Fig. 7 is just off to the side of the body, and is embedded in the turbulent, separated boundary layer that is generated on the side of the vehicle. These curves clearly require a longer averaging interval before the statistics will be smooth. In the wake the agreement is good close to the body but the computed recirculation zone is smaller than in experiments presumably due to the much smaller Reynolds number of the computation and the lack of a viscous ground plane.

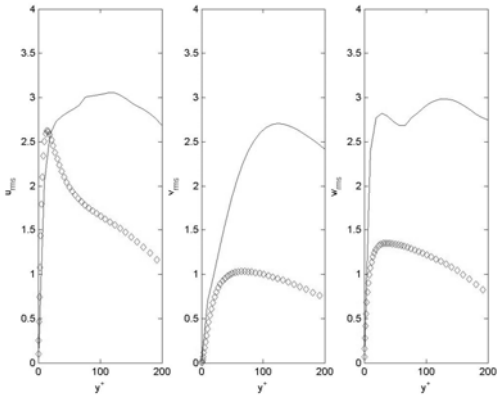

Figure 3. RMS Reynolds stresses at R_e=360,000. ◊, DNS R_θ=500 (Spalart, 1988); —, gridfree scheme.

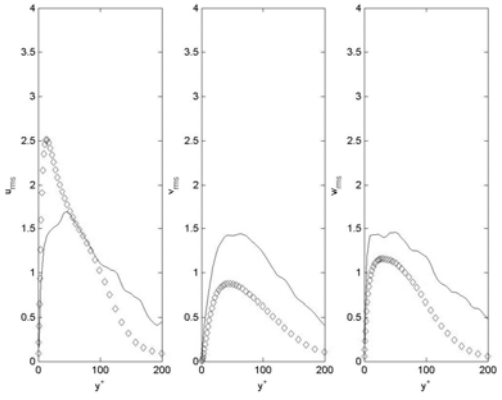

Figure 4. RMS Reynolds stresses at R_e=64,800. ◊, DNS R_θ=300 (Spalart, 1988); —, gridfree scheme.

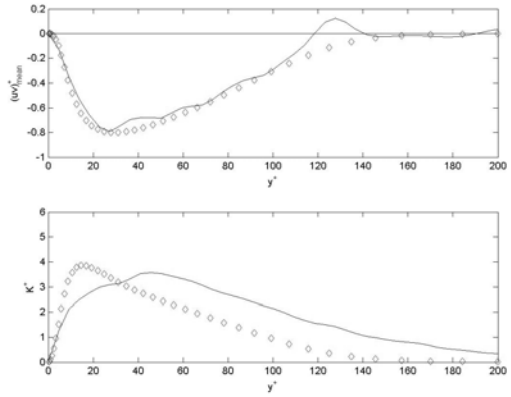

Figure 5. Reynolds shear stress $\overline{uv}^+$ and turbulent kinetic energy at R_e=64,800. ○, DNS R_θ=300 (Spalart, 1988); —, gridfree scheme.

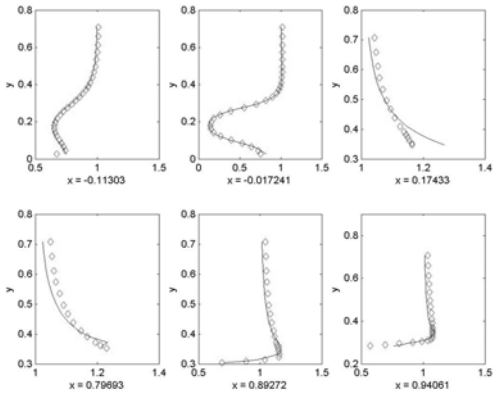

Figure 6. Streamwise velocity on centreline: —, computed; ◊, experiment (Lienhart, et al., 2000).

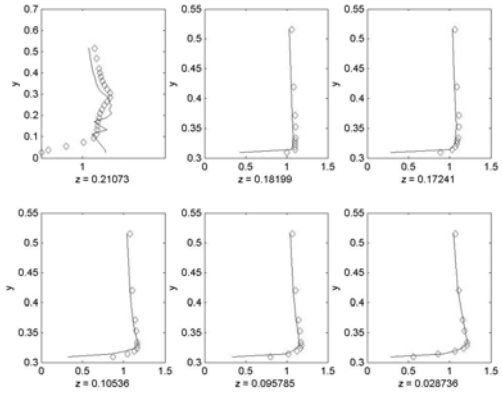

Figure 7. Streamwise velocity at spanwise locations at x = 0.8678: —, computed; ◊, experiment (Lienhart, et al., 2000).

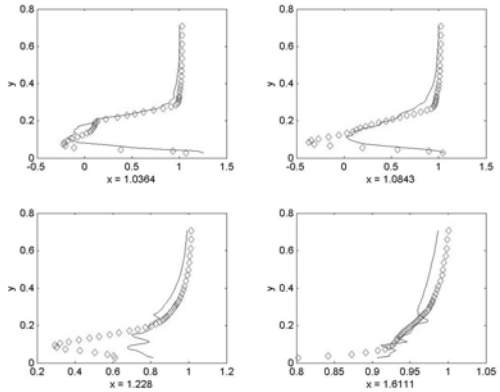

Figure 8. Streamwise velocity on wake centreline: —, computed; ◊, experiment (Lienhart, et al., 2000).

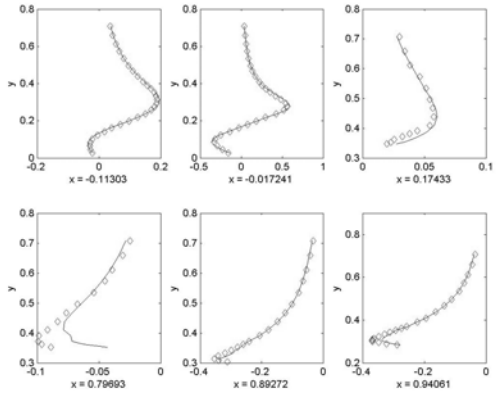

Figure 9. Normal velocity on centerline: —, computed; ◊, experiment (Lienhart, et al., 2000).

Figure 10 compares the predicted turbulent kinetic energy vs. experiment at points along the centerline extending into the wake. The first two locations are over the window and the remaining four are in the wake. Clearly the averaging interval (from time 1 to 1.5) is not long enough to produce fully smooth statistics and this may explain some of the variation in accuracy of the individual curves. In particular, only a few large scale vortices can develop and shed off the body in the averaging time so these have an undue influence on higher order statistics. Nonetheless, some trends appear to be well captured such as the double-peaked distribution in the near wake at x = 1.0364.

3.2 Visualizations

The Lagrangian character of vortex methods provides an opportunity for learning about the properties of turbulent flows via visualizations of the computed field of vortex elements. Shown here are some results for selected flows that illustrate and reveal information about the turbulent physics as well as provide a check on the physicality of the gridfree simulation scheme.

Figure 11 gives a view of the vortices that have formed over the top surface of the Ahmed body looking down from above at t = 1.91 after an impulsive start to the flow. In this example, R_e = 40,000 and there are 28,538 surface triangles. New vortices are seen to be created nearly everywhere on the surface and there are approximately 2.5 million vortex tubes in the flow at this time. The figure reveals the formation of boundary layers from the leading edge, their downstream transition to turbulence, and the formation of turbulent structures. The latter are visible as streamwise agglomerations of vortices as well as the corrugated outer edges of the turbulent boundary layers that form on the sides of the body. Some evidence for the movement of the flow over the sides toward the centerline is visible in streamwise vortical features near the rear window. A fully turbulent boundary layer is in the middle region of the top surface and it is from here that turbulent statistics have been compared to experiment. The consistency of the observed vortical structures with known characteristics of turbulent boundary layers helps to explain the good agreement in predicting velocity statistics shown previously.

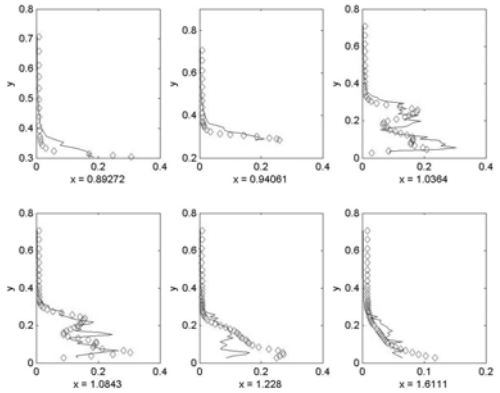

Figure 10. Turbulent kinetic energy at locations on centreline: —, computed; ◊, experiment (Lienhart, et al., 2000).

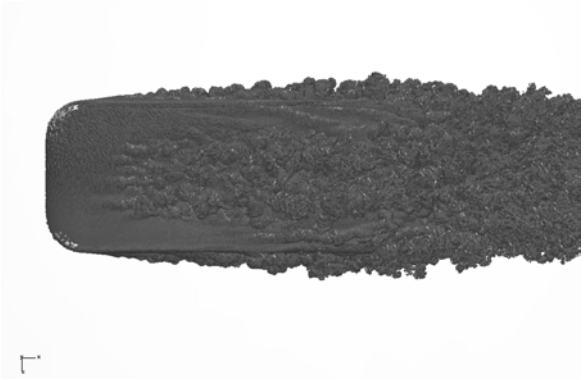

Figure 11. Vortices on the top surface of the Ahmed body.

An ongoing effort concerns the simulation of flow past a sphere under various conditions and Reynolds numbers. The computed vortex tubes at a fixed time for the flow past a sphere with and without rotation at R_e = 40,000 are given in Figs. 12 and 13, respectively. The rotation is counter clockwise around a spanwise axis. The grid resolution is coarse in these cases with the consequence, particularly for the flow in Fig. 12, that the vortex tubes experience significant perturbations that encourage the flow to behave as if it were tripped. In fact, the computed forces and separations for the flow in Fig. 12 agree well with that of a tripped sphere. The rotating sphere has highly unsteady separation along its top with numerous vortices forming and shedding in time. In another example, Fig. 14 shows the complex flow past two spheres arranged one behind the other. It is particularly interesting to note the interaction of

the unsteady wake of the upstream sphere with the downstream sphere. This flow also illustrates one of the attractive properties of the grid free scheme: it is a simple matter to apply the method to complex geometries since only near-wall meshes are required in setting up simulations.

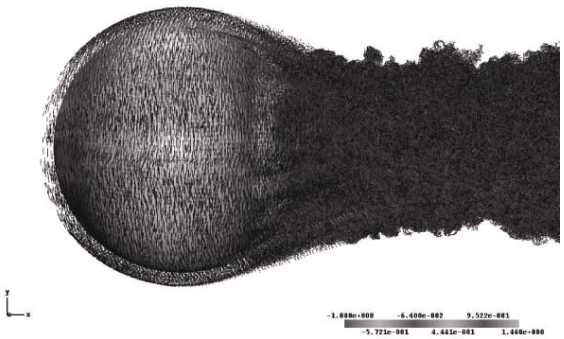

Figure 12. Vortex elements in sphere flow at R_e = 40,000.

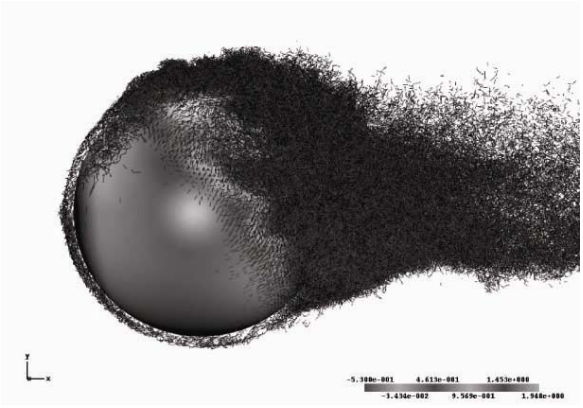

Figure 13. Vortex elements in flow past a counter-clockwise rotating sphere at R_e = 40,000.

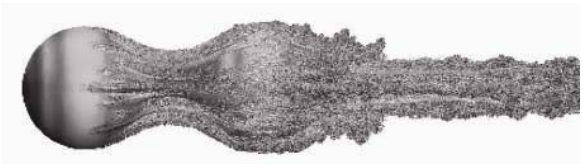

Figure 14. Vortex elements in flow past two spheres at R_e = 500,000.

4. CONCLUSIONS

Some of the capabilities of a gridfree scheme for turbulent flow simulation have been described. These include reasonably accurate predictions of mean velocity fields and a varying capacity for reproducing Reynolds stresses depending most obviously on how well resolved the near-wall triangularizations are for a given flow Reynolds number. A particularly attractive feature of the approach is the opportunity it provides to examine the characteristics of the turbulent vorticity field via visualization of the Lagrangian elements.

Future developments are centered on continuing efforts to improve parallelization of execution and array storage so that problems with $O(10^6)$ prisms and $O(10^7)$ vortex tubes can be computed in a reasonable time frame. This capability should allow for the realistic simulation of turbulent flows with Reynolds numbers of $O(10^6)$ and higher. Though it has not been discussed here, the calculation of pressure is a post-processing step in vortex methods and further work in improving this aspect of the approach is also a current priority.

ACKNOWLEDGEMENT

This research was supported in part by the National Science Foundation through TeraGrid resources provided by PSC, NCSA and SDSC.

REFERENCES

Ahmed, S. R., et al., 1984, Some Salient Features of the Time-Averaged Ground Vehicle Wake, SAE Paper No. 840300.

Bernard, P.S. and Wallace, J.M., 2002, Turbulent Flow: Analysis, Measurement and Prediction, John Wiley & Sons, Inc.

Chorin, A. J., 1993, Hairpin Removal in Vortex Interactions II, Journal of Computational Physics, Vol. 107, pp. 1 - 9.

Chorin, A. J., 1994, Vorticity and Turbulence, Springer-Verlag.

Greengard, L. and Rokhlin, V., 1987, A Fast Algorithm for Particle Simulations, Journal of Computational Physics, Vol. 73, pp. 325-348.

Lienhart, H., Stoots, C. and Becker, S., 2000, Flow and Turbulence Structures in the Wake of a Simplified Car Model (Ahmed model), DGLR Fach. Symp. Der AG STAB, Stuttgart Univ.

Morel, T., 1978, Aerodynamics Drag of Bluff Body Shapes Characteristic of Hatch-Back Cars, SAE Paper 780267.

Puckett, E. G., 1993, `Vortex Methods: An Introduction and Survey of Selected Research Topics, in Incompressible Computational Fluid Dynamics: Trends and Advances, edited by M. D. Gunzburger and R. A. Nicolaides, Cambridge University Press, pp. 335-407.

Spalart, P.R., 1988, Direct Simulation of a Turbulent Boundary Layer Up to R_θ = 1410, Journal of Fluid Mechanics, Vol. 187, pp. 61-98.